Crystallographic preferred orientations and microstructure of a Variscan marble mylonite in the Ossa-Morena Zone (SW Iberia)

I. Romeo [a,*], R. Capote [a], R. Lunar [b]

[a] *Departamento de Geodinámica, Facultad de Ciencias Geológicas, Universidad Complutense de Madrid, 28040 Madrid, Spain*
[b] *Departamento de Cristalografía y Mineralogía, Facultad de Ciencias Geológicas, Universidad Complutense de Madrid, 28040 Madrid, Spain*

Abstract

The mylonitic marbles of the Cherneca shear zone, a Variscan sinistral strike-slip structure developed in the Ossa-Morena Zone (SW Iberia) related to the emplacement of the Santa Olalla Igneous Complex, were studied in detail. Different mylonites (from protomylonites to ultramylonites) were analyzed by Electron Back-Scattering Diffraction (EBSD) in order to determine the crystallographic preferred orientation (CPO) of calcite. The CPOs show very good agreement with experimental torsion work giving suitable interpretations of the operative slip systems and strain quantifications, thus the obtained natural CPOs validate the experimental approaches. A wide range of observed textures and microstructures are mainly controlled by the amount of shear strain, the presence of secondary phases, and the development of antithetic subsidiary shears. The effect of secondary phases and the nucleation of antithetic shear bands on texture development are discussed.

Keywords: Crystallographic preferred orientation; Texture; Microstructure; Mylonite; Shear bands; Variscan Orogeny

1. Introduction

The more suitable rocks for accumulating large amounts of ductile strain at the low temperature dominant conditions in the upper crust are carbonate rocks. Considering their abundance elsewhere, these rocks play a fundamental role during orogenesis. Thus, advancing the knowledge of the formation and evolution of plastic flow in carbonate shear zones is a main objective for the understanding of orogenic processes (Pfiffner, 1982; Van der Pluijm, 1991).

Calcite textures and microstructures in deformed marbles provide information regarding kinematics, deformation mechanisms, stress quantification, characteristics of the strain, and physical parameters during deformation (e.g. temperature). The type of texture (crystallographic preferred orientation, CPO) developed during ductile deformation of calcite is controlled by two factors: active crystallographic slip systems at a given temperature, and the amount of strain. The geological significance of calcite CPOs is shown by experiments carried out on natural marbles (Griggs et al., 1960; Handin et al., 1960; Schmid et al., 1977, 1980; Rutter, 1974, 1995; Rutter et al., 1994; Casey et al., 1998; Pieri et al., 2001a,b; Barnhoorn et al., 2004, 2005), synthetic calcite aggregates (Walker et al., 1990; Barnhoorn et al., 2005), and on simulations performed by numerical modelling (Wenk et al., 1987, 1997, 1998; Wenk and Christie, 1991; Lebensohn et al., 1998; Pieri et al., 2001b). Numerical and experimental results have proven helpful when compared to natural samples.

Deformation experiments on calcite single-crystals (Turner et al., 1954; Griggs et al., 1960; Turner and Heard, 1965; Borg and Handin, 1967; Paterson and Turner, 1970; Weiss and Turner, 1972; Braillon and Serughetti, 1976; Turner and Orozco, 1976; Spiers and Wenk, 1980; De Bresser and Spiers, 1990, 1993) were used to define the crystallographic slip and twin systems active at different temperature, stress and strain rate conditions, and critical activation shear stresses (reviews can be found in Paterson, 1979, and De Bresser and Spiers, 1997). Plastic deformation of calcite occurs in low

* Corresponding author. Fax: +34 91 394 4845.

and high temperature regimes. At low temperature deformation is characterized by twining on e{-1018}<40-41>, slip on r{10-14}<-2021> (r<sd>) and on f{-1012}<2-201> (f<sd>). At high temperature deformation is controlled by slip on r{10-14}<-2021> (r<sd>), f{-1012}<10-11>, c{0001}<-12-10> (c<a>), and r{10-14}<-12-10> (r<a>). Both strain regimes are described in De Bresser and Spiers (1997). The r<a> slip system was postulated later by Pieri et al. (2001a) and Barnhoorn et al. (2004) after large torsion experiments in marbles (although no direct observations on single-crystal deformation have been obtained yet). The results from Barnhoorn et al. (2004) on experimental deformation of Carrara marble are very relevant for analyzing natural ultramylonite samples because, for the first time, steady state conditions were reached during the largest shear strains obtained by torsion. Numerical modelling (Wenk et al., 1987, 1997, 1998) was successfully used to reproduce different CPOs depending on the slips systems considered to be active, with a good agreement with laboratory experiments (Lebensohn et al., 1998; Pieri et al., 2001b).

In this paper, we present a systematic study of the microstructures and CPOs of the Cherneca shear zone, a Variscan sinistral structure developed in the Ossa-Morena Zone (SW Iberia). This structure has a special relevance considering that it is the source of the magmas of the Santa Olalla Igneous Complex (Romeo et al., 2006b) and of the recently discovered magmatic mineralized pipes of the Aguablanca Ni–Cu–PGE ore deposit (Lunar et al., 1997; Ortega et al., 1999, 2004; Tornos et al., 2001; Piña et al., 2006).

Samples were chosen to represent a wide range of total strain within the Cherneca marble shear zone. Samples comprise: (1) ultramylonites completely dominated by dynamically recrystallized grains; (2) mylonites characterized by core-mantle textures with oblique porphyroclasts indicating low amount of shear; and (3) oblique subsidiary antithetic shears developed cross-cutting a zone of protomylonites. We also analyzed textures of the marble out of the shear zone to compare them with textures within shear zone. CPOs were obtained from individual crystallographic orientations of grains measured by Electron Back-Scattering Diffraction (EBSD) (Prior et al., 1999; Leiss et al., 2000).

The obtained CPOs were compared with experimental and numerical modelling studies, which show good agreement. Our results and comparison with experimental and numerical examples provided: (1) the sense of shear for each sample (from patterns with monoclinic symmetry with respect to the shear plane) being coherent with mesoscopic indicators; (2) the slip systems active during deformation, giving a qualitative estimate of temperature in agreement with the proximity of the magmatic intrusions; and (3) a qualitative estimate of the amount of shear accommodated in each sample.

2. Geological setting

The Cherneca shear zone is located on the southern limb of the Olivenza-Monesterio antiform (Fig. 1), a major, WNW–ESE trending Variscan structure, occupying a central position

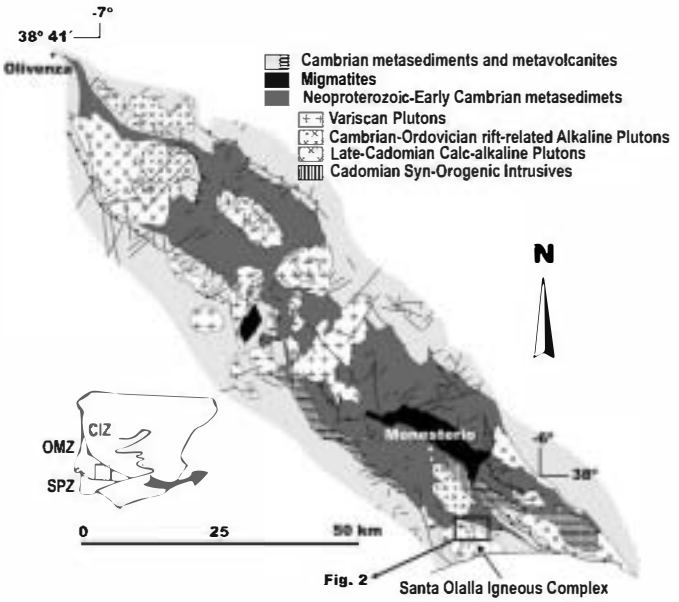

Fig. 1. Geological map of the plutonic rocks in the Olivenza-Monesterio antiform showing the location of the Santa Olalla Igneous Complex and Fig. 2 that corresponds to the Cherneca shear zone. Inset: Southern divisions of the Iberian Massif (CIZ, Central Iberian Zone; OMZ, Ossa-Morena Zone; SPZ, South Portuguese Zone).

within the Ossa-Morena Zone (OMZ). The OMZ forms one of the SW divisions of the Iberian Massif, the westernmost outcrop of the Variscan orogen in Europe (Ribeiro et al., 1990). The OMZ has been interpreted as a poly-orogenic terrane accreted to the Central Iberian Zone during the Cadomian orogeny (620–530 Ma), the suture of which is exposed along the Badajoz-Córdoba shear zone (Quesada, 1990, 1991, 1997; Eguíluz et al., 2000). A rifting event culminating in formation of a new oceanic tract (Rheic Ocean) is recorded in the OMZ during Cambro-Ordovician times (Liñán and Quesada, 1990; Sánchez-García et al., 2003; Expósito et al., 2003). A passive margin stage followed until the onset of the Variscan orogeny in mid Devonian times. In this part of the orogen, Variscan tectonics started with oblique subduction of the Rheic Ocean beneath the southern margin of the OMZ, where accretion/eventual obduction of oceanic fragments formed the Pulo do Lobo accretionary prism and Beja-Acebuches Ophiolite (Munhá et al., 1986; Silva, 1989; Quesada, 1991; Quesada et al., 1994a). At the same time, an arc was growing on the hanging-wall, i.e. on the Ossa-Morena plate (Santos et al., 1987). Subduction of the oceanic crust led to oblique (sinistral) collision against the South Portuguese Zone, which diachronously propagated southeastwards from Late Devonian to Late Viséan (Ribeiro et al., 1990 Quesada, 1991). Subsequent orogenesis consisted of sinistral continental subduction of the outer margin of the South Portuguese Zone under the OMZ until its waning in Early Permian times.

During the whole orogenic process from the Middle Devonian to the Early Permian, the OMZ acted as the upper plate being subjected to a transpressional sinistral tectonic regime. The pre-existing Cadomian suture was reactivated under a sinistral strike-slip regime (Badajoz-Córdoba shear zone). This

structure now constitutes the northern boundary of the OMZ (Ribeiro et al., 1990; Ábalos et al., 1991; Quesada, 1991; Quesada and Dallmeyer, 1994).

Variscan deformation in the OMZ resulted in a thick-skinned, strike-slip duplex structure, generated by the inversion of the horst and graben tectonic compartmentalization acquired during the Cambrian-Ordovician rifting event (Sánchez-García et al., 2003). Internal deformation of each horse is very variable and includes several folding and oblique thrust generations, as well as coeval extensional (transtensional) events. In the case of the Olivenza-Monesterio antiform, the basement was shortened by developing an antiformal stack, which tightened in several steps. The Palaeozoic cover shows four different stages of deformation: (1) The cover initially detached from the basement in a thin-skinned fashion with a SW-verging imbricate fan and large associated recumbent folds (Vauchez, 1975; Quesada et al., 1994b; Expósito, 2000); (2) a transtensional event followed during which some syn-orogenic basins were formed (e.g., the Terena flysch basin); (3) a folding event, also SW-vergent but with steep axial planes, affected the already deformed thin-skinned imbricate fan; and (4) finally the overall NW–SE trend of the orogen was reworked by late sinistral strike-slip faults striking N50–70° that generated the map view sigmoidal shapes that characterized the tectonic structure of the OMZ.

The Cherneca shear zone is a N120 striking structure with a subvertical dip at the terrain level, probably with a listric NE-dip geometry at depth, if we consider the structural pattern showed by the IBERSEIS seismic profile across the Ossa-Morena Zone (Simancas et al., 2003). It is situated in the southern limb of recumbent SW-vergent Olivenza-Monesterio antiform, between the Serie Negra formation and the Bodonal Cala volcanosedimentary complex. The Serie Negra is a Neoproterozoic succession of alternating pyrite-bearing black slate and meta-graywacke with thin intercalations of meta-volcanic rocks and black quartzite (Eguíluz, 1988) that lies in the nucleus of the antiform. The Bodonal-Cala Complex is an Early Cambrian volcano-sedimentary sequence of rhyolite, crystal tuff, fine tuff, cinder slate, and coarse-grained feldspar-phyric rhyolite (Eguíluz, 1988). The Bodonal-Cala Complex also shows intercalations of carbonate rocks, more abundant towards the top where marbles dominate the succession. The presence of the underlying Neoproterozoic Serie Negra at the same level as the Early Cambrian Bodonal Cala Complex suggest a reverse movement for the Cherneca shear zone. Nevertheless the fabrics related to this initial movement are completely reworked by sinistral strike-slip displacement which is the object of this paper.

Towards the SW of the Cherneca shear zone, a group of plutonic rocks, the Santa Olalla Igneous Complex, was emplaced during Variscan times (Eguíluz et al., 1989; Bateman et al., 1992; Romeo et al., 2006a,b). A structural and gravimetric study of the igneous rocks (Romeo et al., 2006b) evidenced that the roots of the plutons are located in the NE margin towards the Cherneca shear zone, indicating that this structure was probably the conduit used by magma to ascent.

The Santa Olalla Igneous Complex is formed by two main plutons: the Santa Olalla stock to the south and the Aguablanca stock to the north (Fig. 2). The Santa Olalla stock (Eguíluz

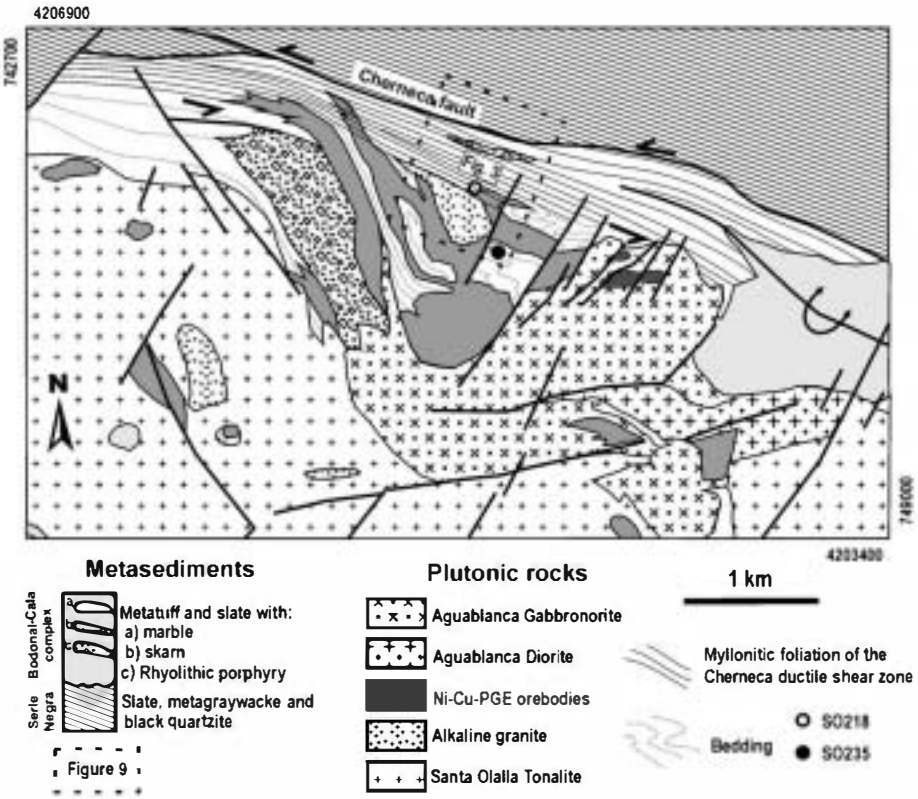

Fig. 2. Geological map of the Cherneca shear zone. The locations of the samples SO218 and SO235, Fig. 3 and Fig. 9 are indicated.

et al., 1989), the largest pluton of the complex, consists of amphibole-biotite quartz-diorite in the northern area grading to dominant tonalitic facies in the centre. The Aguablanca stock is a mafic subcircular pluton composed of phlogopite-rich gabbronorite and norite, grading to diorite to the south. This mafic intrusion has undergone significant endoskarn processes along the northern boundary induced by contact with marbles of the upper part of the Bodonal-Cala Complex (Casquet, 1980). The intrusion of the Santa Olalla Igneous Complex during deformation of the Cherneca shear zone induced a sinistral shear strain that is recorded in the NE half of the complex by magmatic deformation (Romeo et al., 2006b).

The geochronology of the Santa Olalla Igneous Complex yielded a Visean age (U–Pb on zircons, Romeo et al., 2006a), similar to other plutonic intrusions along the Olivenza Monesterio antiform: Brovales (340 ± 4 Ma obtained by Pb–Pb with the thermal evaporation technique (Kober, 1986, 1987) on zircons, Montero et al., 2000), Valuengo (342 ± 4 Ma obtained by Pb–Pb with the thermal evaporation technique on zircons, Montero et al., 2000) and Burguillos del Cerro (330 ± 9 Ma obtained by whole rock Rb–Sr, Bachiller et al., 1997; 335 Ma obtained by Ar–Ar on amphibole, Dallmeyer et al., 1995; 338 ± 1.5 Ma obtained by U–Pb on allanite, Casquet et al., 1998). The activity of Aguablanca stock has been dated from 343 to 338 Ma (U–Pb on zircons, Romeo et al., 2006a).

The study of the Cherneca shear zone has special relevance as it was proposed to be the structure that favoured the emplacement in the Aguablanca stock northern boundary of a Ni–Cu–PGE ore deposit (Lunar et al., 1997; Ortega et al., 1999, 2004; Tornos et al., 1999; Casquet et al., 2001; Tornos et al., 2001; Piña et al., 2006). The mineralization is closely associated with a 70–80° N dipping, funnel-like magmatic breccia (250–300 m wide in the N–S direction and up to 600 m long in the E–W direction). The breccia comprises barren or slightly mineralized mafic-ultramafic cumulate fragments enveloped by hornblende and phlogopite-rich gabbronorite. The gabbronorite contains disseminated and semi-massive Ni–Cu–Fe magmatic sulphides.

The Cherneca shear zone was studied in the northern area of the Aguablanca stock and the Ni–Cu–PGE mineralization. In this area the Cherneca shear zone is developed on the marble of the Bodonal-Cala Complex, which is locally transformed into garnet-rich skarn. The marble and the skarn are both deformed by sinistral shearing, indicating that deformation continued after the dated magmatic event. Strain along the Cherneca shear zone was concentrated in the Bodonal-Cala marble because of its ductile rheology during deformation, rather than on the more fragile Serie Negra. During the cooling period after Variscan orogenesis, the marbles became rheologically stronger and thus the late movements on the shear zone were restricted to the contact between the Bodonal-Cala Complex and the Serie Negra.

3. Field kinematic observations and sample location

The Cherneca shear zone shows typical characteristics of ductile deformation under simple shear, dominated by strain-concentration processes and localized softening. Mylonitization developed an anisotropic and complex shear zone with rock types that range from low-strained protomylonites to highly-strained ultramylonites. Five mylonitic marble samples (SO217A, SO217B, SO217C, SO217D, SO218) were collected for detailed microstructural and textural characterization across the Cherneca shear zone. The results were compared with a marble sample located outside of the shear zone (SO235). The latter is considered to represent the starting material prior to mylonitization. Sample SO218 corresponds to a low-strained mylonite and is located near the southern boundary of the shear zone (Fig. 2). Samples SO217C and SO217D are highly-strained ultramylonites located in the central part of the shear zone (Fig. 3). Samples SO217A and SO217B correspond to antithetic subsidiary shears developed on a protomylonite band (Fig. 3); also located in the central area of the shear zone.

Samples SO218, SO217C and SO217D were cut perpendicular to the mylonitic foliation (XY plane, normal to Z) and parallel to the stretching lineation (X direction) of the main sinistral shear belt. Samples SO217A and SO217B were cut perpendicular to the foliation plane of the subsidiary dextral shear bands (X′Y plane, normal to Z′) and parallel to their lineations (X′ direction). This second coordinate system has a Y axis parallel to the main shear coordinate system and new X′ and Z′ axes that are rotated 25° in respect of the X and Y axes of the main shear (Fig. 3). The angle between the main shear foliation plane and the antithetic shear bands is 25°.

The sinistral kinematics of the Cherneca shear zone are indicated by mesoscopic σ and δ-porphyroclasts and S–C structures on the outcrop. These observations are consistent with the sinistral oblique character of the Variscan orogeny elsewhere in the Ossa-Morena Zone (Eguíluz et al., 2000).

The protomylonite band shown in Fig. 3 is characterized by a weak mylonitic foliation parallel to the main shear. Subsidiary shears cross-cutting the protomylonitic foliation appears, whose kinematics are indicated by dextral drags of the protomylonitic foliation. These subsidiary shears deform the protomylonitic foliation; consequently, they can not correspond to structures formed before the Cherneca Shear Zone. These subsidiary shears are asymptotic relative to the boundaries of the protomylonite band (Fig. 3) in contact with ultramylonites. It can be established from these structural relationships that the subsidiary shears were formed after the protomylonitic foliation but before or simultaneously with the ultramylonitization at the boundaries of the protomylonite band. The drags of the protomylonitic foliation caused by the subsidiary shears clearly indicate a dextral shear sense for these particular structures. The subsidiary dextral shears are rotated 25° clockwise with respect to the main shear.

This structural pattern (Fig. 3) could be interpreted as an S–C′ mesoscale structure implying a contradicting dextral shear criterion for the Cherneca shear zone. This interpretation is against all the shear sense indicators on the outcrop, and also against all the microstructural and crystallographic indicators presented in this contribution, that clearly established a sinistral shear sense for the Cherneca Shear Zone. Thus

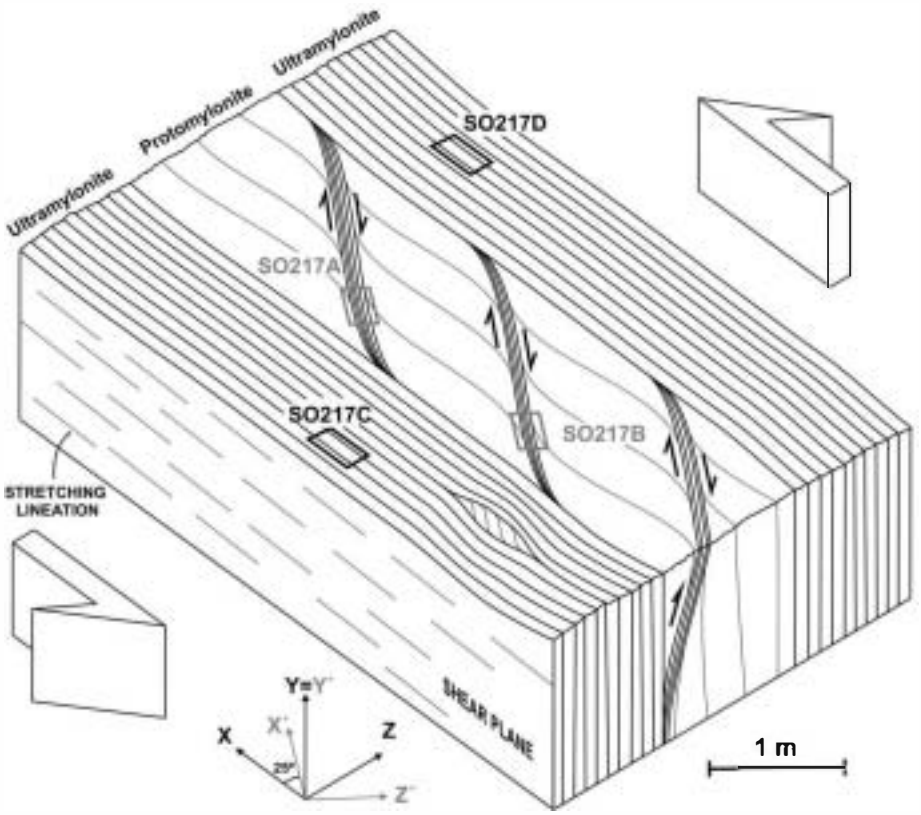

Fig. 3. A scheme of the location of the samples SO217A, SO217B, SO217C and SO217D, two belonging to ultramylonitic bands, and two from antithetic subsidiary shears, indicating the 3D geometry and kinematics. The reference frames used for the main shear samples (XYZ) and for the subsidiary shear samples (X′YZ′) are indicated.

we reject to interpret it as an S–C′ structure, considering that the observed subsidiary dextral shears are antithetic structures, which kinematics serves to accommodate transpressive strain. The formation of antithetic shear bands with orientations similar to C′ shears was noticed by Behrmann (1987), indicating that the interpretation of a subsidiary shears as C′ shears has to be done carefully. The interpretation of the dextral subsidiary shears as antithetic shears developed into a sinistral shear zone, accommodating a transpressive component of strain, is in good agreement with the transpressional character of the Variscan collision in the Ossa-Morena Zone (e.g. Eguíluz et al., 2000).

4. Results

The result of the microtectonic study performed on the mylonitic marble of the Cherneca shear zone is divided in two sections: the description of the microstructures determined by optical microscopy and that of the CPOs determined by EBSD.

4.1. Microstructure

The observed microstructures of the studied samples are described below. The grain sizes were determined by reconstructing grain boundaries from the crystallographic data, considering the presence of a grain boundary when the misorientation angles between adjacent points were higher than 15°. This method allows accurate and easy measurements of average grain sizes considering that the spacing of the crystallographic data was chosen to be at least one-half of the finest grains found in each sample.

4.1.1. Pre-shearing stage (sample SO235)

Bedding of the Bodonal-Cala marble out of the Cherneca shear zone is shown by alternating bands with fine (80 μm) and coarse (250 μm) grains. Calcite grains are equidimensional and have abundant triple junctions and straight grain boundaries. Although a few twins are present, no significant internal deformation occurred.

4.1.2. Low-strained mylonite (sample SO218)

The mineralogy of SO218, a sample located close to the southern boundary of the shear zone, consists of dominant calcite, with minor rounded quartz grains (<1%). The microstructure of SO218 is typical of low-strained mylonite where porphyroclasts (200 μm) are abundant (31%) and appear completely surrounded by dynamically recrystallized grains (10 μm, 69%) producing a core-mantle texture (Fig. 4). A few bent twins were formed in the first stages of deformation and were rotated during further strain towards parallelism with the shear zone boundary. Rotation and stretching of twinned porphyroclasts produced a very strong shape preferred orientation (SPO) with a trend

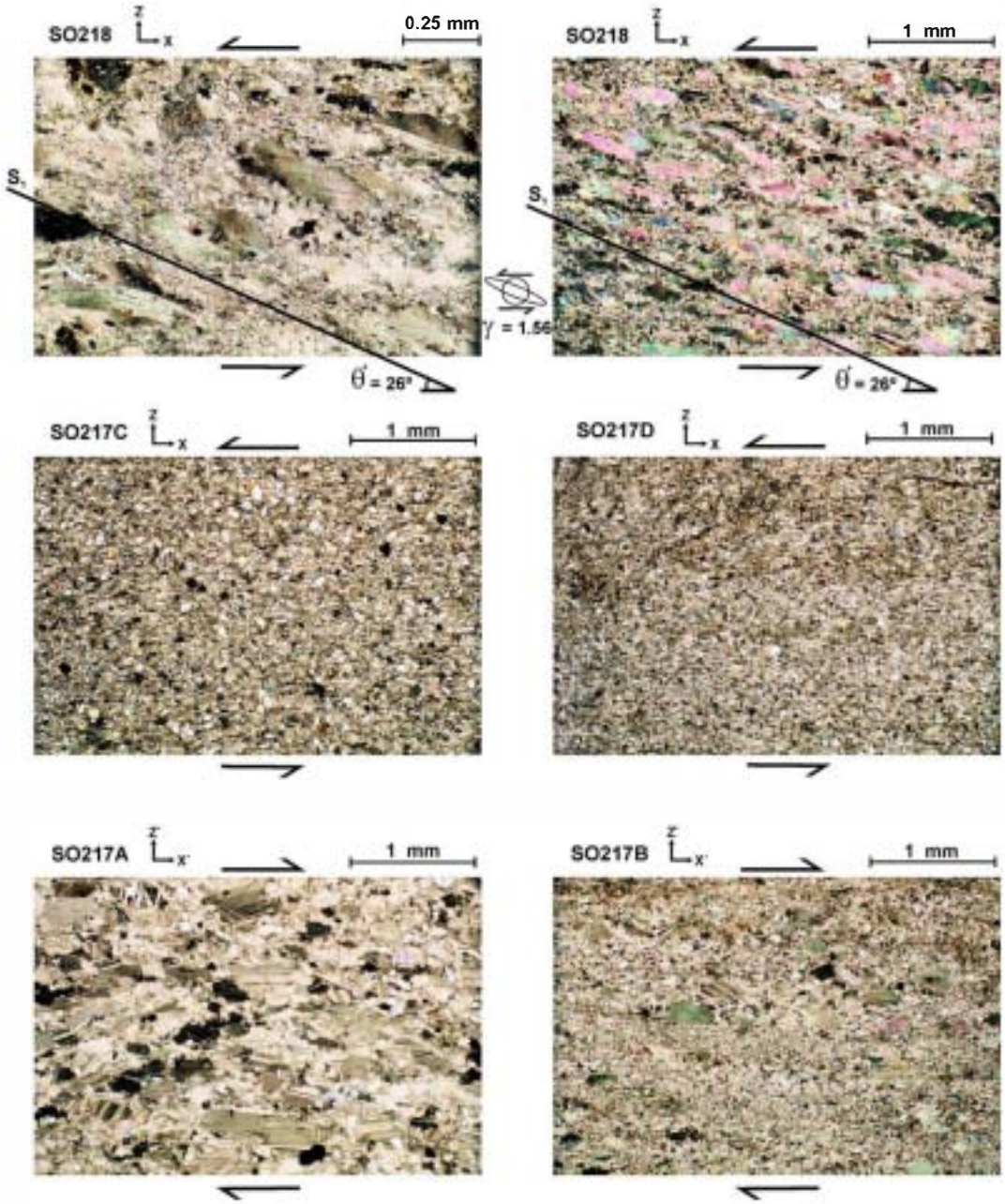

Fig. 4. Microphotographs of SO218, SO217C, SO217D, SO217A, SO217B. The sample SO218 is characterized by a core-mantle recrystallized microstructure, where the elongation of porphyroclasts indicate the presence of a primary oblique foliation S1 that was used to calculate the amount of shear strain (γ). Note the presence of quartz as secondary phase in the ultramylonite samples SO217C and SO217D. The samples of the subsidiary shear bands (SO217A, SO217B) feature a core-mantle texture where the elongation of the porphyroclasts is subparallel to the subsidiary shear plane.

oblique to the shear zone boundary, implying a sinistral shear sense for this sample. All the porphyroclasts of this sample show elliptical shapes with the same orientation of their longer axes (Fig. 4). These grains may have originated from initially rounded grains similar to those of the non-sheared sample (SO235), which acted as initial subcircular passive shear-strain markers that were transformed to ellipses by internal plastic deformation. Thus, we can infer that they are strain ellipses defining an oblique foliation S_1 (following the notation of Barnhoorn et al., 2004). The angle between the long axis of the strain ellipse (parallel to oblique foliation S_1) and the shear plane (θ') can be directly related to the shear strain (γ) by the expression $\tan(2\theta') = 2/\gamma$ (Ramsay and Huber, 1983). In this case θ' is 26° and gives a shear strain of $\gamma = 1.56$ (Fig. 4). This estimation is a maximum considering that the Cherneca shear zone probably has a transpressive component, as will be discussed later. Flattening perpendicular to the shear zone would have decreased θ' overestimating the measured γ value. This kind of oblique core-mantle microstructure has been successfully reproduced by Pieri et al. (2001a,b) and Barnhoorn et al. (2004) during experimental torsion

studies at different temperature conditions for values of $\gamma = 1.5-3$.

4.1.3. Ultramylonites (samples SO217C, SO217D)

Hand-specimens of samples SO217C and SO217D are white marbles, although large percentage of impurities can be found with microscopic analysis (Fig. 4). Secondary rounded quartz grains are present with an abundance of ≈30% in SO217C and ≈20% in SO217D. The average grain size of SO217C is 70 μm for quartz and 30 μm for calcite, in contrast to the smaller average sizes of SO217D, 35 μm for quartz and 25 μm for calcite. In SO217D, boundaries between calcite grains are more sinuous than those of SO217C whose grain boundaries are straighter. SO217D shows thus a complete dynamically recrystallized mosaic texture except for quartz with slightly coarser grain size than calcite. The calcite texture of SO217C is more disturbed by the presence of a larger amount of quartz grains with bigger grain sizes. The presence of coarser and abundant quartz may, therefore, control the average size of calcite grains. This sample shows straighter calcite boundaries, which probably indicates that dynamic recrystallization did not play an important role in the development of the texture. Texture of sample SO217C was probably controlled by internal deformation during dragging of the calcite crystals between quartz grains.

The development of a stable secondary oblique foliation (S_2 following the terminology of Barnhoorn et al., 2004), equivalent to that observed in large-strained and fully recrystallized samples of the experiments performed by Pieri et al. (2001a,b) and Barnhoorn et al. (2004), was not observed in our ultramylonite samples (Fig. 4). The lack of a secondary foliation in SO217C and SO217D may have been caused by the presence of large amounts of quartz grains, inhibiting the formation this microstructure.

4.1.4. Subsidiary antithetic shear bands (samples SO217A, SO217B)

Two subsidiary antithetic shears developed on a protomylonitic band were studied (SO217A, SO217B; Fig. 3). The microstructure of these samples is very different to that of the ultramylonites and the low-strained mylonite. The samples of the subsidiary antithetic shears also show different textures from one another. Both samples feature a core-mantle texture with abundant porphyroclasts surrounded by recrystallized grains, but SO217A shows coarser grains for both porphyroclasts and recrystallized grains than SO217B (Fig. 4). SO217A has an average size of 350 μm for the porphyroclasts and 30 μm for the recrystallized grains, while SO217B shows averages of 200 μm and 25 μm, respectively. The difference between both samples can be related to the intensity of dynamic recrystallization. In SO217A only 44% of its surface was dynamically recrystallized, contrasting with the 77% of surface dominated by recrystallization in SO217B. Consequently, it can be inferred that the shear strain accommodated in the subsidiary shear of SO217B was higher than the shear strain absorbed by SO217A, taking into account that the percentage of recrystallized grains increases with shear strain. The weakening associated to the grain size reduction during dynamic recrystallization was more pronounced in SO217B, allowing a feed-back mechanism that produced strain concentration in this narrow subsidiary shear. The deformation state of SO217A can therefore be considered as an early stage during the generation of a subsidiary shear.

Despite the fact that the subsidiary antithetic shear bands show small displacement in the field (Fig. 3), porphyroclasts in both samples, SO217A and SO217B, show a clear elongation that is oriented subparallel to the subsidiary shear plane. These microstructures contrast with the oblique orientation of the porphyroclasts of similar size in SO218 with respect to the main shear plane. It is widely observed in experimental studies (Pieri et al., 2001a,b; Barnhoorn et al., 2004) that, during deformation, porphyroclasts are passively rotated towards the shear plane, reaching almost complete parallelism at very high shear strains. Considering the small displacements accommodated by the subsidiary shear bands that can be observed in the outcrop (Fig. 3) a very high shear strain must be discarded as the mechanism that generated this SPO parallel to the shear plane in these samples. Thus a different explanation is needed. One possibility is that this SPO could be generated by the general sinistral shear strain in the protomylonitic band, where later the subsidiary dextral shear bands were formed. The observed SPO relative to the main shear reference frame gives a sinistral shear sense that is coherent with mesoscopic indicators. This SPO oblique to the main shear reference frame (S_1) would have acted as a planar anisotropy favouring the nucleation of antithetic subsidiary shears parallel to this previous fabric in order to accommodate the transpressive component of the Cherneca shear zone. This interpretation also yields an explanation for the antithetic shear sense of the subsidiary shear bands.

4.2. Crystallographic preferred orientations (CPOs)

CPOs were determined by individual orientation data of calcite grains obtained by EBSD during automatic mapping of previously prepared samples. The oriented samples were cut in thin sections that were used to study the microstructures under microscope and were polished for EBSD analysis following the techniques described by Prior et al. (1999).

The treatment of orientation data of the mapped area was used to delineate grain boundaries when the misorientation angles between adjacent points were higher than 15°. Using the misorientation analytical method the grain boundaries of the mapped area were reconstructed and the grain size distribution was obtained, allowing to separate the orientation data of different size classes. This methodology was applied to distinguish the different contribution of porphyroclasts and recrystallized grains to the total CPO.

4.2.1. Pre-shearing stage (sample SO235)

The sample SO235 belongs to the Bodonal-Cala marbles outside the Cherneca shear zone. Bedding (alternating layers of fine and coarse grains) shows two folding events at mesoscale. The CPO of the total data set is approximately random indicating that the amount of pure shear accommodated by this

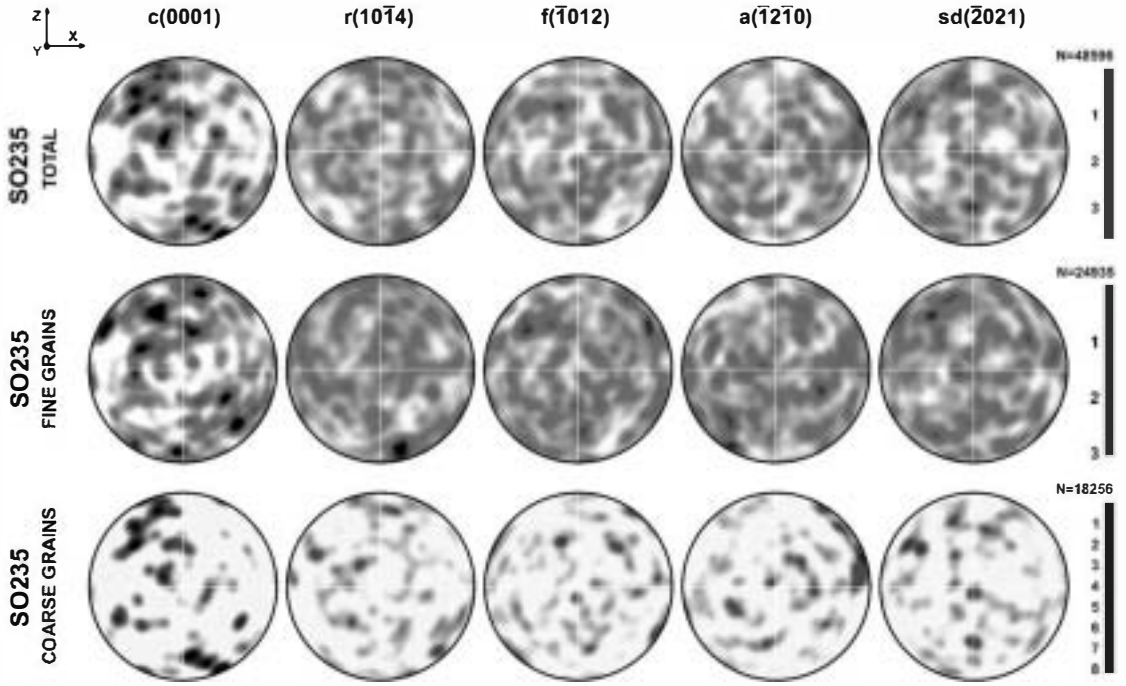

Fig. 5. Equal area lower hemisphere projections of CPOs of SO235, a marble located out of the Cherneca shear zone. The sample is characterized by alternating bands with coarse and fine grains, whose contributions to the total CPO are also shown.

sample during folding did not generate a significant preferred orientation (Fig. 5). This sample is characterized by alternating layers with fine and coarse grains whose crystallographic orientation data were separated by grain boundary reconstruction and grain size analysis, which gave very similar random CPOs for both (Fig. 5).

4.2.2. Low-strained mylonite (sample SO218)

Despite moderate shearing as indicated by the microstructure of SO218 (Fig. 4), a strong CPO was developed during deformation (Fig. 6). It is characterized by a maximum of the {c} poles perpendicular to the shear plane accompanied with a weaker girdle of {c} poles in the YZ

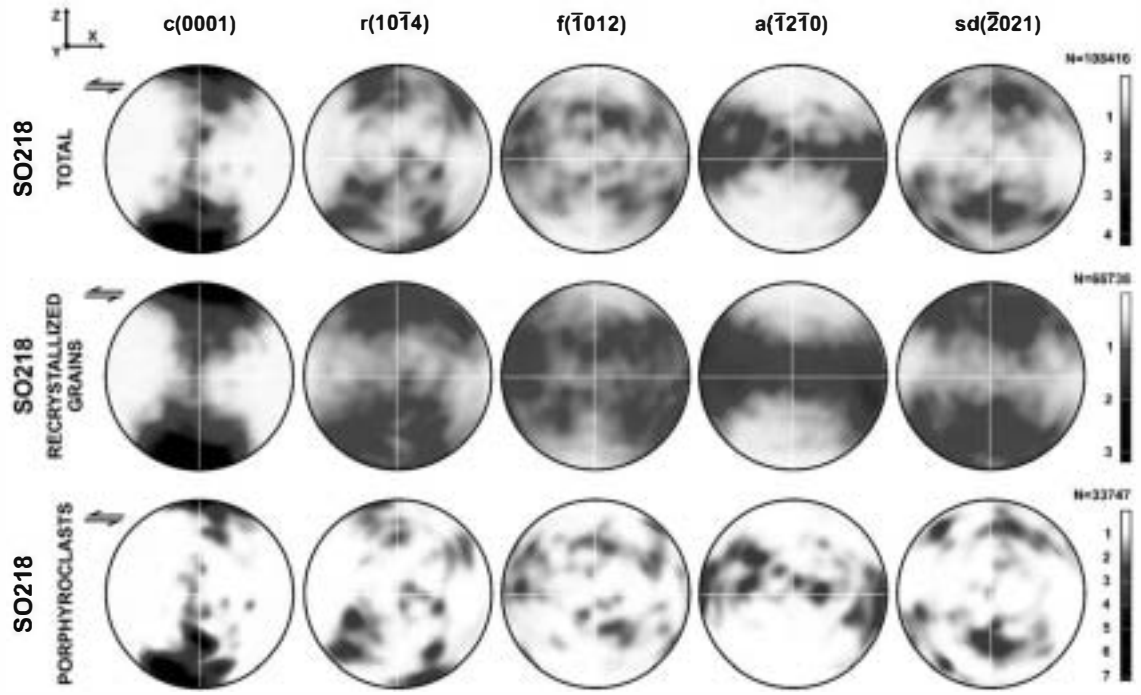

Fig. 6. Equal area lower hemisphere projections of CPOs of SO218, a low-strained mylonite. The total CPO was separated showing the preferred orientation of the recrystallized grains and the porphyroclasts.

plane. The <a> axes are distributed within a girdle in the XY shear plane with a clear maximum in the X direction. This disposition seems to indicate that slip on {c}<a> was active during deformation. The CPO symmetry is monoclinic (10° of clockwise rotation) with respect to the shear plane indicating a sinistral sense of shear, in agreement with outcrop indicators.

The CPOs of the dynamically recrystallized grains and the porphyroclasts are not completely equivalent. The more homogeneous data distribution in the CPO of the recrystallized grains relative to the CPO of the porphyroclasts may be due to the difference of number of grains measured. Some important differences in the CPOs can be observed. Although the distribution of {c} poles and <a> axes is almost equivalent, the {r} poles pattern is different. On one hand, the recrystallized grains show a wide maximum of {r} poles in Z, indicating that the slip system r<a> proposed by Pieri et al. (2001a,b) and Barnhoorn et al. (2004) could be active during deformation. On the other hand, the {r} poles of the porphyroclasts show two clusters: one rotated 10° with respect to the Z axis in concert with the sense of shear and the other one rotated 50° with respect to the Z axis opposite to the sense of shear.

4.2.3. Ultramylonites (samples SO217C, SO217D)

The ultramylonite samples, SO217C and SO217D belong to different ultramylonite bands (Fig. 3) and yielded different CPOs (Fig. 7), probably controlled by the different amounts of quartz grains in each sample.

SO217C shows a monoclinic CPO with a maximum of {c} poles giving a sinistral sense of shear for this sample in agreement with the general kinematics of the shear zone. The <a> axes are disposed within a weak girdle perpendicular to the main {c} maximum and show three prominent clusters within the shear plane (XY). The {r} pole plot displays three maxima, one parallel to the maximum of {c} poles and the other two maxima disposed with a monoclinic symmetry with respect to the shear plane (XY). The most suitable slip system that can be deduced from this CPO is c<a>.

The CPO obtained for SO217D, which is a fully recrystallized sample, shows an orthorhombic symmetry with respect to the shear plane, with a wide maximum of {c} and {r} poles normal to the shear plane (XY). The <a> axes are disposed within the shear plane with a higher abundance in the X direction. This geometry suggests that both c<a> and r<a> could have been active during deformation. c<a> is possibly the dominant slip system as deduced from this CPO, because the {c} maximum is stronger than the {r} one in the Z direction normal to the shearing foliation.

4.2.4. Subsidiary antithetic shear bands (samples SO217A, SO217B)

A detailed CPO study was performed to unravel the evolution of the texture in subsidiary shear bands. Two subsidiary antithetic shear bands located in a protomylonite band were analyzed by EBSD. Their CPOs are shown in Fig. 8. All the diagrams are referred to the previously described X′YZ′ coordinate system, which corresponds to the subsidiary shear plane (X′Y normal to Z′) and slip direction (X′). The orientation of the coordinate system of the general shear (XYZ) is also shown in Fig. 8 in order to help the interpretation.

Sample SO217B shows a complex CPO which is the mixture of two different CPOs, the orientation of the recrystallized matrix and the porphyroclasts. The recrystallized grains show a wide maximum of the {c} poles perpendicular to the subsidiary shear plane and a weaker maximum in the same place of the {r} poles. In contrast, the <a> axes are oriented in a girdle within the subsidiary shear plane (X′Y), with a cluster close to the shear direction (X′). Similarly to SO217D (within the ultramylonites of the main shear zone), the recrystallized grains of SO217B show an orthorhombic symmetry that indicates that c<a> and to lesser degree r<a> were the active slip systems.

The orientation of the porphyroclasts in SO217B is not equivalent to that of the recrystallized grains. The disposition of {c} poles is also around Z′ but in this case two different maxima can be distinguished, one in Z (note that it is the axis normal the foliation plane of the main shear) and the other one between Z and X. The orientation of <a> axes is restricted

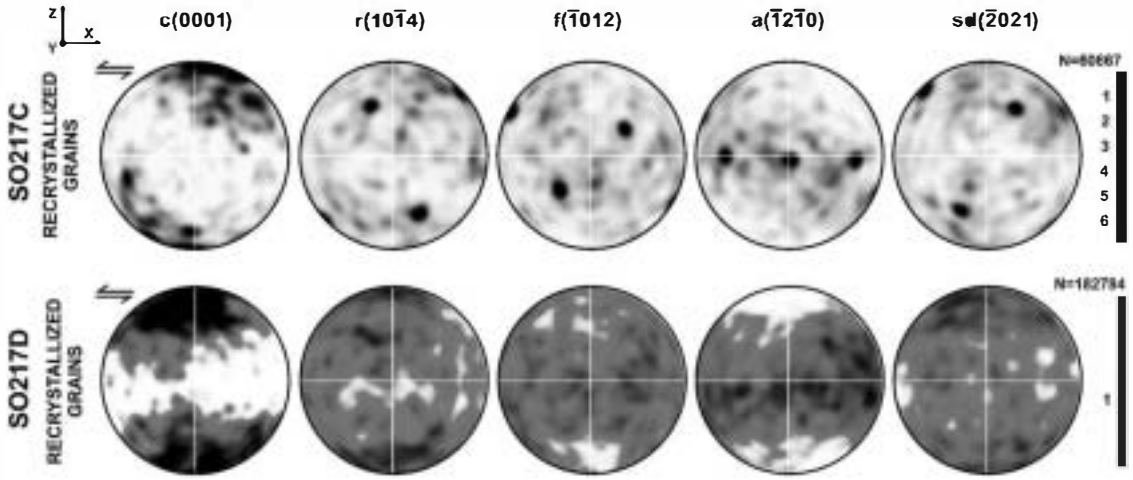

Fig. 7. Equal area lower hemisphere projections of CPOs of the ultramylonite samples SO217C and SO217D.

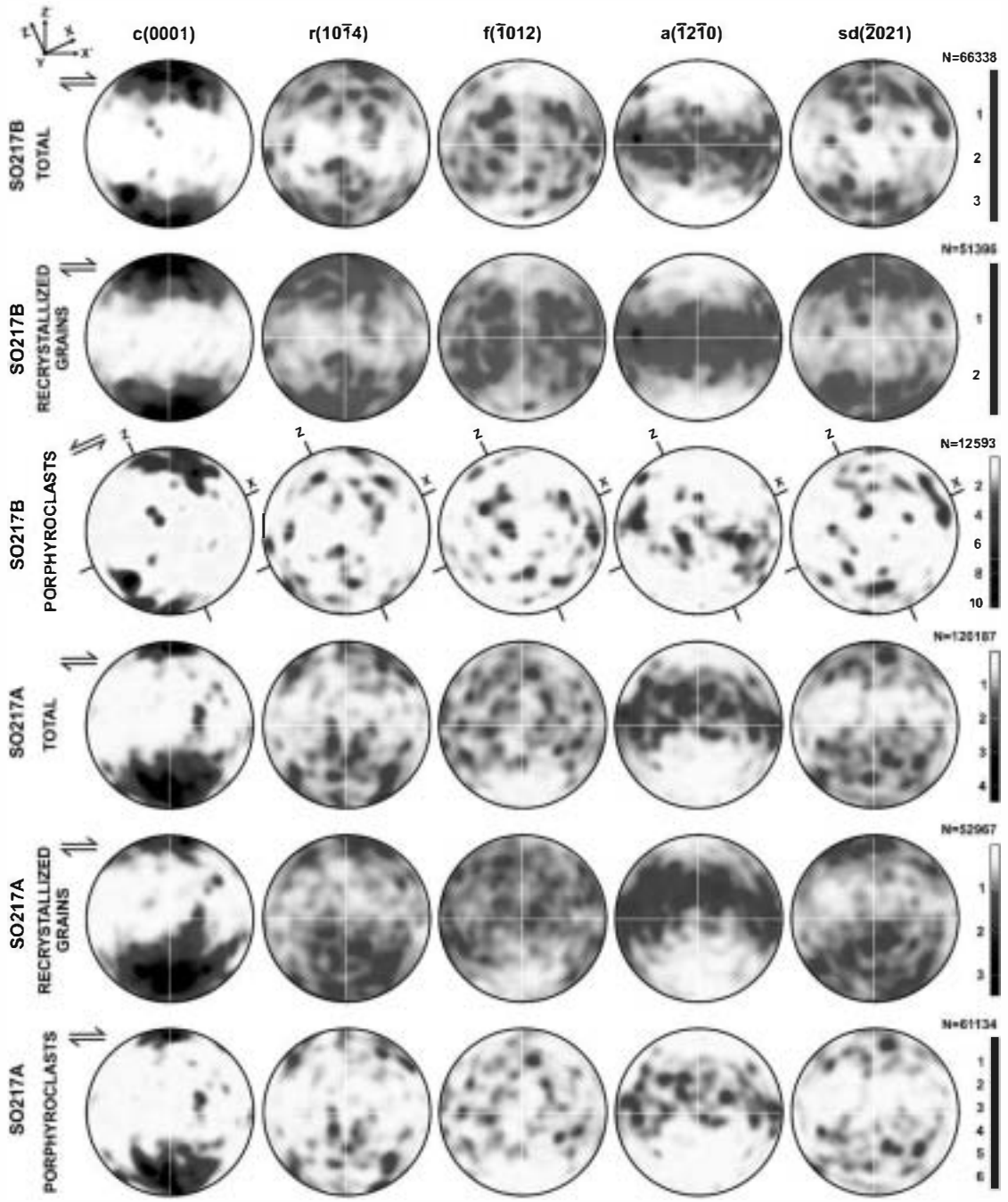

Fig. 8. Equal area lower hemisphere projections of CPOs of the antithetic subsidiary shear bands, SO217A and SO217B. In both samples the contribution to the total CPOs of the recrystallized grains and the porphyroclasts was discriminated. The reference frame of the subsidiary shear bands plus the reference frame of the main shear are indicated to help the interpretation of relict fabrics in the porphyroclasts of SO217B.

to a girdle perpendicular to the secondly described {c} maximum, showing also three clusters inside this girdle. If we analyze this CPO relative to the reference system of the general shear (XYZ), it shows a monoclinic symmetry indicating a sinistral sense of shear. The most favoured slip systems for this CPO are c<a>, r<a> and also r<sd>.

The CPOs from both the recrystallized grains and the porphyroclasts in sample SO217A are equivalent, and are similar to the CPO from the recrystallized grains of SO217B. There is a small rotation of SO217A (10°) in the Z′Y plane probably due to small error in the orientation of the cutting plane during sample preparation. Beside this difference, the CPO of this sample is similar to the CPO of the recrystallized grains of SO217B, and thus we interpret that the same slip systems were active during deformation: c<a> and to lesser degree r<a>.

5. Discussion

The deformation observed across the Cherneca shear zone is in the plastic regime. Although some mechanical twins

are observed (Fig. 4) the amount of shear strain that can be accommodated by twining is very small ($\gamma_{max} = 0.68$, considering the optimum single-crystal orientation, Wenk, 1985). This, together with the observations of undulatory extinction, subgrains and recrystallized grains (core-mantle textures; Fig. 4), indicate that internal plastic deformation of calcite was dominantly generated by slip and climb of dislocations. The core-mantle microstructure of SO218 (Fig. 4) shows very similar sizes of subgrains and recrystallized grains, suggesting that subgrain rotation was the main process leading to dynamic recrystallization.

5.1. Comparison of the CPO results with experimental works and numerical simulations

Although previous experimental studies were performed in simple shear (Schmid et al., 1977; Kern and Wenk, 1983), more complete data record was obtained from the torsion setup, allowing very large shear strains at different temperature conditions (Casey et al., 1998; Pieri et al., 2001a,b; Barnhoorn et al., 2004, 2005). This experimental work is the main data set used to compare our results on natural samples. Generally, our natural samples show textures equivalent to those of the experiments, although natural samples often display weaker CPOs with wider maxima. This could be related to a certain degree of thermal annealing (Barnhoorn et al., 2005) after deformation, a process that would be favoured by contact metamorphism associated to the Aguablanca gabbronorite.

5.1.1. Low-strained mylonite (sample SO218)

A similar CPO to that of sample SO218 was obtained in the experiments performed by Barnhoorn et al. (2004) for the samples with $\gamma = 2$–5 and 727 °C. However in our case the maximum are wider and less defined. This softening of the CPO could be related to thermal annealing. Thermal annealing of experimentally deformed samples of Carrara marble (Barnhoorn et al., 2005) caused a dispersion of the CPO pattern that is very similar to the CPO of recrystallized grains in SO218 (Carrara marble deformed at $\gamma = 5$ and 1 h of annealing; Barnhoorn et al., 2005). Values of $\gamma = 2$–5 are near to the results obtained from the analysis of the microstructure (Fig 4) where the sheared porphyroclasts act as passive markers giving a strain value of $\gamma = 1.56$ (see the microstructure description of SO218). This sample is located close to the southern boundary of the Cherneca shear zone where the marbles are moderately sheared.

CPOs with monoclinic symmetry indicative of sinistral shear sense have been observed in porphyroclasts and recrystallized grains of sample SO218. This monoclinic symmetry is more pronounced in porphyroclasts than in recrystallized grains. This latter CPO is close to an orthorhombic symmetry (Fig. 6). This discrepancy can be explained by the different deformation processes that occur in both types of grains. The consumption of grains by grain boundary migration during dynamic recrystallization generates a continuous resetting of the fabric, which allows for the preservation of an orthorhombic symmetry of the CPO. However, the porphyroclasts undergo continuous internal deformation and rotation during shearing which produces a monoclinic CPO. A similar explanation was proposed for monoclinic versus orthorhombic symmetries in grey and white mylonites, respectively, by Herwegh and Kunze (2002). The presence of nano-scale particles in the grain boundaries of grey mylonites causes slower grain boundary migration, which favours the conservation of a monoclinic symmetry. In contrast, the continuously recrystallized texture of the white mylonites generates an orthorhombic symmetry.

5.1.2. Ultramylonites (samples SO217C, SO217D)

The CPO obtained for SO217C is equivalent to that obtained by Barnhoorn et al. (2004), for samples deformed at 500–600 °C and $\gamma = 2$–4. This complex CPO has been reproduced (Pieri et al., 2001b) using the numerical model of Wenk et al., 1987, which assumes that {c}<a> and {r}<s> slip systems are active at the same time. Similar CPOs were also obtained during experimental studies on calcite by Schmid et al., 1977, and in naturally deformed samples (Behrmann, 1983; Dietrich and Song, 1984; Ratschbacher et al., 1991; Herwegh and Kunze, 2002) where the asymmetry of the {c} maximum relative to the shear plane has been extensively applied as a shear sense indicator.

In contrast to SO217C, sample SO217D displays a CPO with an orthorhombic symmetry that has been observed in other studies on natural marbles deformed under simple shear (Busch and Van der Pluijm, 1995; Bestmann et al., 2000; Herwegh and Kunze, 2002). Orthorhombic symmetry is typical of completely recrystallized microstructures where a continuous resetting of the fabric takes place by grain boundary migration. This weak CPO differs from samples deformed in laboratory (Pieri et al., 2001a,b; Barnhoorn et al., 2004) but it is similar to the results of Barnhoorn et al. (2005) obtained by annealing of a previously deformed ($\gamma = 5$) Carrara marble.

5.1.3. Subsidiary antithetic shear bands (samples SO217A, SO217B)

The recrystallized grains of SO217B (antithetic shear band) and the complete data set of SO217A (antithetic shear band) both yielded a CPO with an orthorhombic symmetry equivalent to that from SO217D (main sinistral shear), although each sample has its own coordinate system. The dextral subsidiary shear bands are developed across a protomylonitic band. The CPOs of SO217B and SO217A show deformation in these subsidiary shears in a direction that is 25° in clockwise sense with respect to the main shear plane. The calcite grains are fully reoriented during deformation along the subsidiary shear bands, so in these bands the CPO has an orthorhombic symmetry with respect to the subsidiary shear plane. The same comparisons with previous studies as those done with SO217D can be applied to these samples.

In contrast with the orthorhombic symmetry obtained for the recrystallized grains, the porphyroclasts of SO217B yielded an asymmetric preferred orientation that, when considered relative to the main shear (XYZ), is equivalent to the experimental samples of Barnhoorn et al. (2004) deformed at 500–600 °C and $\gamma = 4$. This sample shows a CPO equivalent to that of SO217C, indicating the same sinistral shear sense for the main shear.

5.2. *Main shearing versus antithetic shear bands*

In order to understand the role of coarser grains (porphyroclasts) in antithetic shears, we analyzed the geometry of these subsidiary shear bands. The thickness of the shear bands that are characterized by a total dynamically recrystallized microstructure is 1–4 cm. In the surroundings of the recrystallized band, a coarser microstructure formed by porphyroclasts dominates. These coarser grains were strained during sinistral deformation of the main shear on the protomylonite band. The mylonitic foliation in this protomylonite band was dragged in the surroundings of the subsidiary dextral shears (Fig. 3). These folds caused by dragging constitute a flanking structure (Hudleston, 1989; Passchier, 2001; Grasemann and Stüwe, 2001) that is classified as an a-type (antithetic sense) flanking fold with normal drag, which means a drag coherent with the movement of the subsidiary shear, following the classification of Grasemann et al. (2003).

S●217A corresponds to the central zone of recrystallized grains, where porphyroclasts are into this recrystallized band. For this reason S●217A shows for both recrystallized grains and porphyroclasts an orthorhombic symmetry with respect to the subsidiary shear reference frame. However, S●217B corresponds to a thinner subsidiary shear and the thin section comprises part of the recrystallized band and part of the external protomylonite. Consequently, the CP● of the recrystallized grains of S●217B has an orthorhombic symmetry with respect to the subsidiary shear plane (X′Y), while the CP● of the porphyroclasts (that were deformed by the main sinistral shear in the protomylonite) has a monoclinic symmetry with respect to the main shear plane (XY), comparable with experimental results.

The development of these antithetic subsidiary shears serves to accommodate a component of shortening normal to the main shear zone. It also allows the stretching of a more competent band, such as the protomylonite band, where the antithetic shears were found. This tectonic pattern can be described as an initial stage of asymmetric boudinage, developed on this more competent layer, and accomplished by a domino pattern (Goscombe and Passchier, 2003), coherent with the sinistral shear displacement of the main shear zone. The presence of these antithetic subsidiary shears is indicative of an important transpressional component of the Cherneca shear zone, which is in agreement with the general transpressive character of the Variscan orogen elsewhere in the Ossa-Morena Zone (Eguíluz et al., 2000). Deformation across the Cherneca ductile shear zone seems to be partitioned: the sinistral simple shear component is mainly accommodated by ultramylonite bands where strain is concentrated, while the pure shear component of strain is accommodated by subsidiary antithetic shears developed on protomylonite bands.

5.3. *Effect of secondary phases*

The influence of secondary phases on the rheology of rocks was investigated by several authors (e.g. Urai et al., 1986; Drury and Urai, 1990; Olgaard, 1990; Herwegh and Kunze, 2002; Krabbendam et al., 2003). The rheology of a rock with secondary phases can be weaker or stronger than the pure aggregate. In some cases, growing of grains is reduced by pinning caused by secondary phases. When the final grain size is smaller than the steady state recrystallized grain size of the pure aggregate, the material gets softer in the grain size sensitive field (Olgaard, 1990; Herwegh and Kunze, 2002). If secondary phases cause a dragging of the contacts between grains, a reduction of the recrystallization rate occurs, which generates a stronger material behaviour (Walker et al., 1990; Herwegh and Kunze, 2002).

The effect of dragging calcite grain boundaries is increased with the abundance of impurities and also with more anisotropic shapes of the secondary phases (Herwegh and Berger, 2004). In our samples the main secondary phase present is quartz, which appears as rounded clasts floating in a calcite pure matrix (see S●217C in Fig. 4). The isotropic shapes of the quartz grains minimized their effect on rheology, but their abundance was enough to affect the deformation mechanisms. The effect of the abundance of quartz is evidenced by the discrepancy between the CP●s of the samples belonging to the ultramylonitic bands (S●217C, S●217D). S●217C with ≈30% of quartz grains and an average grain size of 70 μm shows a monoclinic CP●. In contrast, S●217D with ≈20% of quartz grains and an average grain size of 35 μm shows an orthorhombic CP● characterized by maxima of {c}and {r} poles parallel to Z. The presence of bigger and more abundant quartz grains in S●217C is enough to strongly affect the texture development. In this sample the role of dynamic recrystallization is reduced by the presence of quartz, that generates drag in the calcite–calcite boundary migration, reducing drastically the recrystallization rate. This process favours the deformation of calcite grains by internal plastic strain (dislocation creep) causing a monoclinic CP● during rotation of calcite grains towards parallelism with the shear plane. S●217D, a similar ultramylonite, is less affected by the presence of second phases and has undergone a fully dynamic recrystallization texture which yielded an orthorhombic CP●.

Although the presence of different amounts of quartz is the preferred explanation for the differences observed between the textures of both ultramylonite samples, a different amount of shear strain due to concentration of deformation could also have played a role. The amount of dynamic recrystallization increases with strain (Pieri et al., 2001a,b; Barnhoorn et al., 2004) causing a subsequent change of the CP● with increasing strain. In this case, S●217C would represent a low-strained sample prior to recrystallization and S●217D a high-strained fully recrystallized sample.

6. Conclusions

The microstructural and textural analyses performed on naturally deformed marble mylonites of the Cherneca Shear Zone indicate a wide range of textures and microstructures within the same shear zone (summarized in Fig. 9). Similar drastic variations in the microstructure and texture at

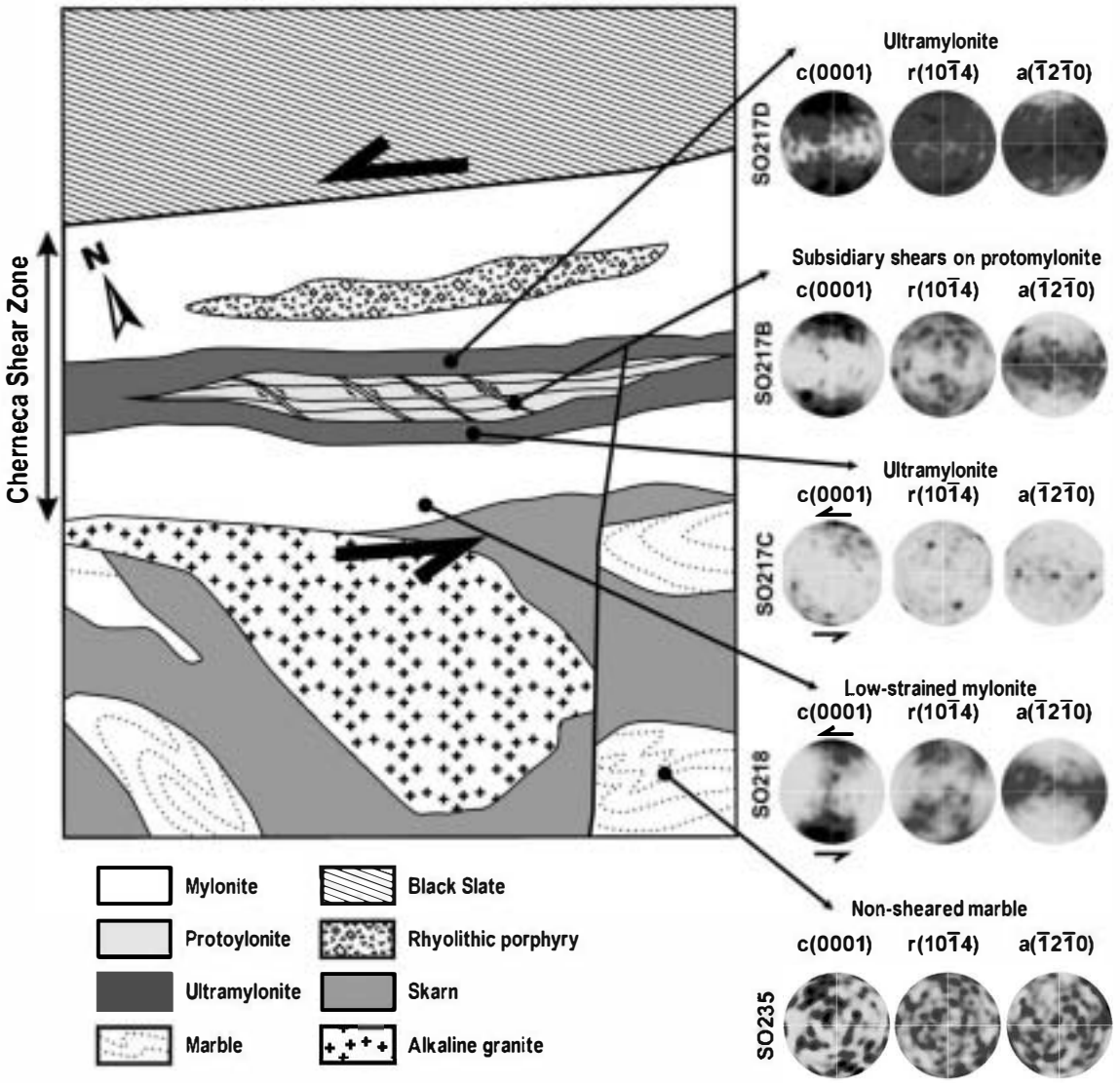

Fig. 9. Geological scheme indicating the main results of the CPO study obtained across the Cherneca shear zone. All the CPOs are plotted within the main shear reference frame, except SO217B which is plotted in respect of the subsidiary shear reference frame. The location of this map is indicated in Fig. 2.

microscopic scale were observed by Busch and Van der Pluijm (1995) in natural mylonites. The comparison of the observed CPOs of different strained mylonites across the Cherneca Shear Zone shows a good agreement with the CPOs obtained both in torsion experiments (Casey et al., 1998; Pieri et al., 2001a,b; Barnhoorn et al., 2004, 2005) and numerical simulations (Wenk et al., 1987, 1997, 1998; Pieri et al., 2001b), which gives support to the application of the experimental approaches and numerical simulations to natural samples. This kind of comparisons allows to establish the active slip systems, the shear sense, and to estimate the amount of strain.

The main factors that control the development of CPOs in the Cherneca shear zone are: (1) the amount of shear strain (γ) that was irregularly distributed across the shear zone due to strain concentration and weakening of the initial protolithic texture; (2) the concentration and grain size of secondary phases that hindered the development of dynamic recrystallization; and (3) the formation of subsidiary antithetic shears that caused rotation of the reference frame and inversion of the sense of shear. The latter caused total resetting of the fabric in some cases and partial resetting in others (where the initial deformation of the general shear persists in the porphyroclasts preferred orientation), depending on the amount of shear accommodated in the subsidiary shear bands.

All the studied samples were mainly controlled by slip on c<a>, a slip system that is only active at high temperatures. This observation is supported by high temperatures expected in the metamorphic aureole of the Aguablanca gabbronorite where these samples were collected. The CPOs with monoclinic symmetry with respect to the shear plane (SO217C in Fig. 7, and SO217B in Fig. 8), indicate that the active slip systems during deformation were c<a> and r<sd> and probably r<a> (Pieri et al., 2001b). At higher shear strains dynamic recrystallization dominated and the slip system r<sd> became inactive. In this case the texture was only controlled by c<a>; probably combined with r<a> (Pieri et al., 2001a,b;

Barnhoorn et al., 2004). For the first time on natural samples, the proposed slip system r<a> has been interpreted that was active during texture development.

A general sinistral shear sense of the Cherneca shear zone is shown by different indicators. Its strike-slip character supports the hypothesis that the Cherneca shear zone may be a favourable conduit for the emplacement of the Santa Olalla Igneous Complex. The presence of releasing bends in the trace of the Cherneca shear zone could open subvertical conduits used by magma ascent (Romeo et al., 2006b), including the mineralized pipes of the Ni–Cu–PGE Aguablanca ore.

Acknowledgements

The research has been supported by Spanish grant PB98-0815. P. Villamor is gratefully thanked for a revision of the manuscript. The comments and suggestions of T.G. Blenkinsop and Ben van der Pluijm greatly improved the manuscript quality. We would also like to thank, Nicola Cayzer, School of GeoSciences, University of Edinburgh, for the management during the EBSD analyses. Mike Hall is thanked for his time and effort in preparing the samples for EBSD.

References

Ábalos, B., Gil Ibarguchi, I., Eguíluz, L., 1991. Cadomian subduction/collision and variscan transpression the Badajoz-Córdoba Shear Belt (SW Spain). Tectonophysics 199, 51–72.

Bachiller, N., Galindo, C., Darbyshire, D.P.F., Casquet, C., 1997. Geocronología Rb-Sr de los leucogranitos del complejo plutónico de Burguillos del Cerro (Badajoz). Geogaceta 21, 29–30.

Barnhoorn, A., Bystricky, M., Burlini, L., Kunze, K., 2004. The role of recrystallization on the deformation behaviour of calcite rocks: larg strin torsion experiments on Carrara marble. Journal of Structural Geology 26, 885–903.

Barnhoorn, A., Bystricky, M., Burlini, L., Kunze, K., 2005. Post-deformational annealing of calcite rocks. Tectonophysics 403, 167–191.

Bateman, R., Martin, M.P., Castro, A., 1992. Mixing of cordierite granitoid and piroxene gabbro, and fractionation, in the Santa Olalla tonalite (Andalucía). Lithos 28, 111–131.

Behrmann, J.H., 1983. Microstructure and fabric transitions in calcite tectonites from the Sierra Alhamilla (Spain). Geologische Rundschau 72, 605–618.

Behrmann, J.H., 1987. A precautionary note on shear bands as kinematic indicators. Journal of Structural Geology 9, 659–666.

Bestmann, M., Kunze, K., Matthews, A., 2000. Evolution of a calcite marble shear zone complex on Thassos Island, Greece: microstructural and textural fabrics and their kinematic significance. Journal of Structural Geology 22, 1789–1807.

Borg, I., Handin, J., 1967. Torsion of calcite single crystals. Journal of Geophysical Research 72, 641–669.

Braillon, P., Serughetti, J., 1976. Deformation plastique de monocristaux de calcite en compression suivant <001>. Physica Status Solidi (a), 36.

Busch, J.P., Van der Pluijm, B.A., 1995. Calcite textures, microstructures and rheological properties of marble mylonites in the Bancroft shear zone, Ontario, Canada. Journal of Structural Geology 17, 677–688.

Casey, M., Kunze, K., Olgaard, D.L., 1998. Texture of Solnhofen limestone deformed to high stains in torsion. Journal of Structural Geology 20, 255–267.

Casquet, C., 1980. Fenómenos de endomorfismo, metamorfismo y metasomatismo en los mármoles de la Rivera de Cala (Sierra Morena). Doctoral Thesis, Universidad Complutense de Madrid. Spain, Madrid, 290 pp.

Casquet, C., Galindo, C., Darbyshire, D.P.F., Noble, S.R., Tornos F., 1998. Fe-U-REEmineralization at Mina Monchi, Burguillos del Cerro, SW Spain. Age and isotope (U–Pb, Rb-Sr and Sm-Nd) constraints on the evolution of the ores: GAC-MAC-APGGQ Quebec '98 Conf. Abstract, 23, A-28.

Casquet, C., Galindo, C., Tornos, F., Velasco, F., Canales, A., 2001. The Aguablanca Cu-Ni ore deposit (Extremadura, Spain), a case of synorogenic orthomagmatic mineralization: age and isotope composition of magmas (Sr,Nd) and ore (S). Ore Geology Reviews 18, 237–250.

Dallmeyer, R.D., García Casquero, J.L., Quesada, C., 1995. Ar/Ar mineral age constraints on the emplacement of the Burgillos del Cerro Igneous Complex (Ossa-Morena Zone, SW Iberia). Boletin Geologico y Minero 106, 203–214.

De Bresser, J.H.P., Spiers, C.J., 1990. In: Knipe, R.J., Rutter, E.H. (Eds.), Deformation Mechanisms Rheology and Tectonics. High temperature deformation of calcite single crystals by r+ and f+ slip, 54. Geological Society of London Special Publications, pp. 285–298.

De Bresser, J.H.P., Spiers, C.J., 1993. Slip systems in calcite single crystals deformed at 300-800 C. Journal of Geophysical Research 98, 6397–6409.

De Bresser, J.H.P., Spiers, C.J., 1997. Strength characteristics of the r, f, and c slip systems in calcite. Tectonophysics 272, 1–23.

Dietrich, D., Song, H., 1984. Calcite fabrics in natural shear environment, the Helvetic nappes of Switzerland. Journal of Structural Geology 6, 19–32.

Drury, M.R., Urai, J.L., 1990. Deformation-related recrystallization processes. Tectonophysics 172, 235–253.

Eguíluz, L., 1988, Petrogénesis de rocas ígneas y metamórficas en el antiforme Burguillos-Monesterio, Macizo Ibérico meridional: PhD, Universidad del Pais Vasco.

Eguiluz, L., Carracedo, M., Apalategui, O., 1989. Stock de Santa Olalla de Cala (Zona de Ossa-Morena, España). Stvdia Geologica Salmanticensia 4, 145–157.

Eguíluz, L., Gil Ibarguchi, J.I., Ábalos, B., Apraiz, A., 2000. Superposed Hercynian and Cadomian orogenic cycles in the Ossa Morena Zone and related areas of the Iberian Massif. Geological Society America Bulletin 112, 1398–1413.

Expósito, I., 2000. Evolucion estructural de la mitad septentrional de la Zona de Ossa-Morena, y su relacion con el límite Zona de Ossa-Morena/Zona Centroibérica. PhD thesis, Universidad de Granada, 296 pp.

Expósito, I., Simancas, J.F., González Lodeiro, F., Bea, F., Montero, P., Salman, K., 2003. Metamorphic and deformational imprint of Cambrian-Lower Ordovician rifting in the Ossa-Morena Zone (Iberian Massif, Spain). Journal of Structural Geology 25, 2077–2087.

Goscombe, B.D., Passchier, C.W., 2003. Asymmetric boudins as shear sense indicators-an assessment from field data. Journal of Structural Geology 25, 575–589.

Grasemann, B., Stüwe, K., 2001. The development of flanking folds during simple shear and their use as kinematic indicators. Journal of Structural Geology 23, 715–724.

Grasemann, B., Stüwe, K., Vannay, J.C., 2003. Sense and non-sense of shear in flanking structures. Journal of Structural Geology 25, 19–34.

Griggs, D.T., Turner, F.J., Heard, H.C., 1960. Deformation of rocks at 500-800C. Memoirs of the Geological Society of America 79, 39–105.

Handin, J., Higgs, D.V., O'Brien, J.K., 1960. Torsion of Yule marble under confining pressure. Memoirs of the Geological Society of America 79, 245–274.

Herwegh, M., Berger, A., 2004. Deformation mechanisms in second-phase affected microstructures and their energy balance. Journal of Structural Geology 26, 1483–1498.

Herwegh, M., Kunze, K., 2002. The influence of nano-scale second-phase particles on deformation of fine grained calcite mylonites. Journal of Structural Geology 24, 1463–1478.

Hudleston, P.J., 1989. The association of folds and veins in shear zones. Journal of Structural Geology 11, 949–957.

Kern, H., Wenk, H.R., 1983. Calcite texture development in experimentally induced ductile shear zones. Contributions to Mineralogy and Petrology 83, 231–236.

Kober, B., 1986. Whole-grain evaporation for $^{207}Pb/^{206}Pb$-age-investigations on single zircons using a double-filament thermal ion source. Contributions to Mineralogy and Petrology 93, 482–490.

Kober, B., 1987. Single-zircon evaporation combined with Pb^+ emitter bedding for $^{207}Pb/^{206}Pb$-age investigations using thermal ion mass spectrometry, and implications to zirconology. Contributions to Mineralogy and Petrology 96, 63–71.

Krabbendam, M., Urai, J.L., Van Vliet, L.J., 2003. Grain size stabilisation by dispersed graphite in a high-grade quartz mylonite: an example from Naxos (Greece). Journal of Structural Geology 25, 855–866.

Lebensolm, R.A., Wenk, H.R., Tomé, C.N., 1998. Modelling deformation and recrystallization textures in calcite. Acta Mater 46, 2683–2693.

Leiss, B., Ullemeyer, K., Weber, K., Passchier, C., 2000. Textures and physical properties of rocks. Journal of Structural Geology 22, 1527–1873.

Liñán, E., Quesada, C., 1990. Ossa-Morena zone: rift phase (Cambrian). In: Dallmeyer, R.D., Martínez-García, E. (Eds.), Pre-Mesozoic Geology of Iberia. Springer-Verlag, Berlin-Heidelberg. Germany, pp. 259–266.

Lunar, R., Ortega, L., Sierra, J., GarcíaPalomero, F., Moreno, T., Prichard, H., 1997. Ni-Cu (PGM) mineralization associated with mafic and ultramafic rocks: the recently discovered Aguablanca ore deposit, SW Spain. In: Papunen, H. (Ed.), Mineral Deposits. Balkema, Rotterdam, pp. 463–466.

Montero, P., Salman, K., Bea, F., Azor, A., Exposito, I., González Lodeiro, F., Martínez Poyatos, D., Simancas, J.F., 2000. New data on the geochronology of the Ossa-Morena Zone, Iberian Massif. In Variscan-Appalachian dynamics: the building of the Upper Paleozoic basement. Basement Tectonics 15, 136–138.

Munhá, J., Barriga, F.J.A.S., Kerrich, R., 1986. High ^{18}O ore-forming fluids in volcanic hosted base metal massive sulphide deposits: geologic $^{18}O/^{16}O$ and D/H evidence for the Iberian Pyrite Belt; Crandon Wisconsin, and Blue Hill, Maine. Economic Geology 81, 530–552.

Olgaard, D.L., 1990. The role of second phase in localizing deformation, in: Knipe, R.J., Rutter, E.H. (Eds.), Deformation Mechanisms, Rheology and Tectonics. Geological Society Special Publication 54, 175–181.

Ortega, L., Moreno, T., Lunar, R., Prichard, H., Sierra, J., Bomati, O., Fisher, P., García Palomero, F., 1999. Minerales del grupo del platino y fases asociadas en el depósito de Ni-Cu-(EGP) de Aguablanca, SO España. Geogaceta 25, 155–158.

Ortega, L., Lunar, R., García-Palomero, F., Moreno, T., Martín Estevez, J.R., Prichard, H.M., Fisher, P.C., 2004. The Aguablanca Ni-Cu-PGE Deposit, Southwestern Iberia: Magmatic ore-forming processes and retrograde evolution. The Canadian Mineralogist 42, 325–335.

Passchier, C.W., 2001. Flanking structures. Journal of Structural Geology 23, 951–962.

Paterson, M.S., 1979. Deformation mechanisms in carbonate crystals. In: Borland, D.W., Clarebrough, L.M., Moore, A.J.W. (Eds.), Physics of Materials. Dept of Mining and Metallurgy, University of Melbourne, pp. 199–208.

Paterson, M.S., Turner, F.J., 1970. Experimental deformation of constrained crystals of calcite in extension. In: Paulitsch, P. (Ed.), Experimental and Natural Rock Deformation. Proceedings International Symposium, Darmstadt, 1969. Springer, Berlin, pp. 109–141.

Pfiffner, O.A., 1982. Deformation mechanisms and flow regimes in limestones from the Helvetic zone of the Swiss Alps. Journal of Structural Geology 4, 429–442.

Pieri, M., Burlini, L., Kunze, K., Stretton, I., Olgaard, D.L., 2001a. Rheological and microstructural evolution of Carrara marble with high shear strain: results from high temperature torsion experiments. Journal of Structural Geology 23, 1393–1413.

Pieri, M., Kunze, K., Burlini, L., Stretton, I., Olgaard, D.L., Burg, J.-P., Wenk, H.-R., 2001b. Texture development of calcite by deformation and dynamic recrystallization at 1000 K during torsion experiments of marble to large strains. Tectonophysics 330, 119–140.

Piña, R., Lunar, R., Ortega, L., Gervilla, F., Alapieti, T., Martínez, C., 2006. Crystal fractionation and sulphide segregation processes in the source chamber of the Aguablanca Ni-Cu-PGE deposit (SW Spain). Economic Geology 101, 865–881.

Prior, D.J., Boyle, A.P., Brenker, F., Cheadle, M.C., Day, A., López, G., Peruzzo, L., Potts, G.J., Reddy, S., Spiess, R., Timms, N.E., Trimby, P., Wheeler, J., Zetterström, L., 1999. The application of electron backscatter diffraction and orientation contrast imaging in the SEM to textural problems in rocks. American Mineralogist 84, 1741–1759.

Quesada, C., 1990. Precambrian successions in SW Iberia: their relationship to Cambrian orogenic events. In: D'Lemos, R.S., Strachan, R.A., Topley, C.G. (Eds.), The Cadomian Orogeny. Geological Society, London, pp. 353–362. 51.

Quesada, C., 1991. Geological constraint on the Paleozoic tectonic evolution of tectonostratigraphic terranes in Iberian Massif. Tectonopysics 185, 225–245.

Quesada, C., 1997. Evolución geodinámica de la Zona Ossa-Morena durante el ciclo Cadomiense. In: Araujo, A., Pereira, M.F. (Eds.), Estudo sobre a geología da Zona de Ossa-Morena (Maciço Ibérico).Livro de Homenagem ao Prof. Univ. de Évora, Francisco Gonçalves, pp. 205–230.

Quesada, C., Dallmeyer, R.D., 1994. Tectonothermal evolution of the Badajoz-Cordoba shear zone (SW Iberia): characteristics and $^{40}Ar/^{39}Ar$ mineral age constraints. Tectonophysics 231, 195–213.

Quesada, C., Fonseca, P.E., Munha, J., Oliveira, J.T., Ribeiro, A., 1994a. The Beja-Acebuches Ophiolite (Southern Iberia Variscan fold belt): geological characterization and geodynamic significance. Boletin Geologico y Minero 105, 3–49.

Quesada, C., Cueto, L.A., Fernández, F.J., Larrea, F.J., 1994b. Mapa Geológico de España, escala 1:50.000, hoja 895: Encinasola. Instituto Geominero de España, pp. 104.

Ramsay, J.G., Huber, M., 1983. The Techniques of Modern Structural Geology. Academic Press, London, 1307 pp.

Ratschbacher, L., Wenk, H.R., Sintubin, M., 1991. Calcite textures: examples form nappes with strain-partitioning. Journal of Structural Geology 13, 369–384.

Ribeiro, A., Quesada, C., Dallmeyer, R.D., 1990. Geodynamic evolution of the Iberian Massif. In: Dallmeyer, R.D., Martínez García, E. (Eds.), Premesozoic Geology of Iberia. Springer, Heidelberg, pp. 339–409.

Romeo, I., Lunar, R., Capote, R., Quesada, C., Dunning, G.R., Piña, R., Ortega, L., 2006a. U/Pb age constraints on Variscan Magmatism and Ni-Cu-PGE metallogeny in the Ossa-Morena Zone (SW Iberia). Journal of the Geological Society of London 163, 837–846.

Romeo, I., Capote, R., Tejero, R., Lunar, R., Quesada, C., 2006b. Magma emplacement in transpression: the Santa Olalla Igneous Complex (Ossa-Morena Zone, SW Iberia). Journal of Structural Geology 28, 1821–1834.

Rutter, E.H., 1974. The influence oftemperature, strain rate and interstitial water in the experimental deformation of calcite rocks. Tectonophysics 22, 311–334.

Rutter, E.H., 1995. Experimental study of the influence of stress temperature and strain on the dynamic recrystallization of Carrara marble. Journal of Geophysical Research 100, 24651–24663.

Rutter, E.H., Casey, M., Burlini, L., 1994. Preferred crystalplastis orientation development during the plastic and superplastic flow of calcite rocks. Journal of Structural Geology 16, 1431–1446.

Sánchez-García, T., Bellido, F., Quesada, C., 2003. Geodynamic setting and geochemical signatures of Cambrian-Ordovician rift-related igneous rocks (Ossa-Morena Zone, SW Iberia). Tectonophysics 365, 233–255.

Santos, J.F., Mata, J., Gonçalves, F., Munhá, J., 1987. Contribuição para o conhecimento geológico-petrológico da região de Santa Súzana: O complexo Vulcanosedimentar da Toca da Moura. Com. Serv. Geol. Portugal 73, 29–48.

Schmid, S.M., Boland, J.N., Paterson, M.S., 1977. Superplastic flow in fine grained limestone. Tectonphysics 43, 257–291.

Schmid, S.M., Paterson, M.S., Boland, J.N., 1980. High temperature flow and dynamic recrystallization in Carrara Marble. Tectonophysics 65, 245–280.

Silva, J.B., 1989. Estrutura de uma geotransversal da Faixa Piritosa: Zona do Vale do Guadiana. Univ. Lisboa, Tese de Doutoramento, 450 pp.

Simancas, J.F., Carbonell, R., González Lodeiro, F., Pérez Estaún, A., Juhlin, C., Ayarza, P., Kashubin, A., Azor, A., Martínez Poyatos, D., Almodóvar, G.R., Pascual, E., Sáez, R., Expósito, I., 2003. Crustal structure of the transpressional Variscan orogen of SW Iberia: SW Iberia deep seismic reflection profile (IBERSEIS). Tectonics 22, 1062.

Spiers, C.J., Wenk, H.R., 1980. Evidence for slip on r and f in the positive sense in deformed calcite single crystals. EOS. Transactions American Geophysical Union 61, 1128.

Tornos, F., Casquet, C., Galindo, C., Canales, A., Velasco, F., 1999. The genesis of the variscan ultramafic-hosted magmatic Cu-Ni deposit of

Aguablanca, SW Spain. In: Stanley, et al. (Eds.), Mineral Deposits: Processes to Processing. Balkema, Rotterdam, pp. 795–798.

Tornos, F., Casquet, C., Galindo, C., Velasco, F., Canales, A., 2001. A new style of Ni-Cu mineralization related to magmatic breccia pipes in a transpressional magmatic arc, Aguablanca, Spain. Mineralium Deposita 36, 700–706.

Turner, F.J., Heard, H.C., 1965. Deformation in calcite crystals at different strain rates. University of California Publications of Geological Science 46, 103–126.

Turner, F.J., Orozco, M., 1976. Crystal bending in metamorphic calcite, and its relations to associated twining. Contributions to Mineralogy and Petrology 57, 83–97.

Turner, F.J., Griggs, D.T., Heard, H.C., 1954. Experimental deformation of calcite crystals. Geological Society of America Bulletin 65, 883–934.

Urai, J.L., Means, W.D., Lister, G.S., 1986. Dynamic recrystallization of minerals. In: Hobbs, B.E., Heard, H.C. (Eds.), Mineral and Rock Deformation: Laboratory Studies—The Paterson Volume. Geophysical Monographs 36, pp. 161–199.

Van der Pluijm, B.A., 1991. Marble mylonites in the Bancroft shear zone, Ontario, Canada: microstructures and deformation mechanisms. Journal of Structural Geology 13, 1125–1135.

Vauchez, A., 1975. Tectoniques tangéantielles superposées dans le segment hercynien Sud-Ibérique: les nappes et plis couchés de la région d'Alconchel-Fregenal de la Sierra (Badajoz). Boletin Geológico y Minero 86, 573–580.

Walker, A.N., Rutter, E.H., Brodie, K.H., 1990. Experimental study of grain-size sensitive flow of synthetic, hot-pressed calcite rocks. In: Knipe, R.J., Rutter, E.H. (Eds.), Deformation Mechanisms, Rheology and Tectonics.. Geological Society Special Publications 54 Geological Society of London, pp. 259–284.

Weiss, L.E., Turner, F.J., 1972. Some observations on translation gliding and kinking in experimentally deformed calcite and dolomite. In: Geophysical Monographs 16. American Geophysical Union. 95–107.

Wenk, H.R., 1985. Carbonates. In: Wenk, H.R. (Ed.), Preferred Orientation in Deformed Metals and Rocks. An Introduction to Modern Texture Analysis. Academic Press, San Diego, pp. 361–384.

Wenk, H.R., Christie, J.M., 1991. Comments on the interpretation of deformation textures in rocks. Journal of Structural Geology 13, 1091–1110.

Wenk, H.R., Takeshita, T., Bechler, E., Erskine, B.G., Matthies, S., 1987. Pure shear and simple shear calcite textures. Comparison of experimental, theoretical and natural data. Journal of Structural Geology 9, 731–745.

Wenk, H.R., Canova, G.C., Brechet, Y., Flandin, L., 1997. A deformation-based model for recrystallization of anisotropic materials. Acta Materia 45, 3285–3296.

Wenk, H.R., Matthies, S., Donovan, J., Chateigner, D., 1998. BEARTEX, a windows-based program system for quantitative texture analysis. Journal of Applied Crystallography 31, 262–269.